A. Ressler et al., From Bio-waste to Bone Substitute…, *Chem. Biochem. Eng. Q.*, **34** (2) 59–71 (2020)

59

From Bio-waste to Bone Substitute: Synthesis of Biomimetic Hydroxyapatite and Its Use in Chitosan-based Composite Scaffold Preparation

A. Ressler,[*] A. Gudelj, K. Zadro, M. Antunović, M. Cvetnić, M. Ivanković, and H. Ivanković

[a]Faculty of Chemical Engineering and Technology, University of Zagreb, HR-10001 Zagreb, Marulićev trg 19, p.p.177, Croatia

Nanocomposite structure of the bone can be mimicked by chitosan/hydroxyapatite (CS/HAp) composite scaffold. Biological hydroxyapatite (HAp) contains various ions, which have a crucial role in bone growth. The aim of the present work was to synthesize biomimetic hydroxyapatite and prepare composite scaffolds based on chitosan, where HAp was synthesised from hen eggshells, seashells and cuttlefish bone. The powders were composed of nano-structured calcium deficient HAp and amorphous calcium phosphate (ACP). In the as-prepared powders, Sr^{2+}, Mg^{2+} and Na^+ ions were detected as a result of using biogenic precursor of Ca^{2+} ions. Highly porous CS/HAp structures have been prepared by freeze-gelation technique. The CS/HAp scaffolds have shown highly porous structure with very well interconnected pores and homogeneously dispersed HAp particles. The MTT assay of CS/HAp scaffolds has shown no toxicity, and the *live*/*dead* assay has confirmed good viability and proliferation of seeded cells.

Keywords:

biogenic source, chitosan, hydroxyapatite, scaffold, trace element

1. Introduction

Considering the improvement of people's living standard and increased life expectancy, it is crucial to develop scaffolds for bone tissue engineering that fulfil various requirements such as bioactivity, biocompatibility, cell-scaffold adhesion, mechanical properties, and biodegradability[1,2]. A promising way to obtain appropriate scaffold is to mimic the structure, element content, and phase composition of natural bone tissue[3–5].

Human bone consists of 65–70 % inorganic phase (calcium phosphates and trace elements), 20–25 % of organic phase (primarily collagen), and 5–8 % of water[6]. Hydroxyapatite ($Ca_{10}(PO_4)_6(OH)_2$, HAp) is a calcium phosphate highly used in bone tissue engineering as scaffold, filler, drug delivery system, and bioactive coating, due to its bioactivity, osteoinductivity, biocompatibility, and chemical similarity to the mineral phase of bone tissue[1,7,8]. Biological HAp in its structure contains various trace elements, such as CO_3^{2-}, Mg^{2+}, Na^+, K^+, Zn^{2+}, Sr^{2+}, Cl^-, F^-, which have a crucial role in bone growth[9,10]. Incorporation of mentioned ions in synthetic HAp crystal lattice can affect its crystallinity, morphology, lattice parameters, thermal stability, solubility, and phase composition, which can significantly improve the biological properties of synthetic HAp bioceramics[11].

Numerous methods have been developed for the synthesis of HAp, such as solid-state, mechano-chemical, chemical precipitation, sol-gel, and hydrothermal methods, using various precursors of calcium and phosphate ions. However, in synthetic stoichiometric HAp there are no trace elements in its structure, which is why natural biogenic sources as potential materials for synthesis of biomimetic HAp have been investigated[1,6,12]. Calcium-rich sources, such as eggshells, seashells, animal bones, cuttlefish bone, and corals represent a promising future of bioceramics because they naturally contain trace elements in their crystal lattice[13]. Additionally, using natural biogenic sources for HAp synthesis, bio-waste (e.g. eggshells, fish bones) is reduced and recycled, and it is considered as an environmentally friendly approach[14,15].

Scaffolds used as biomaterials for bone regeneration should promote cell-cell and cell-material interactions, cell adhesion, extracellular matrix deposition, diffusion of gases, nutrients, and regulatory factors to ensure cell proliferation and differentiation at degradation rate close to regeneration rate of bone tissue, without causing an inflammatory reaction[16]. Combination of HAp and organic phase (biodegradable polymer) leads to improved biologi-

[*]Corresponding author: Antonia Ressler, Tel: +385 1 4597 210, e-mail: aressler@fkit.hr

cal and mechanical properties of composite material. HAp provides bioactivity and osteoinductivity, while polymer provides mechanical resistance, flexibility, and biodegradability[17]. Polymers can enable porous structure, which promotes bone tissue ingrowth and interactions between an implant and natural bone tissue[18]. One promising candidate as polymer matrix in composite scaffolds for bone tissue engineering is biopolymer chitosan (CS). The CS is a naturally occurring polysaccharide obtained from biopolymer chitin by the deacetylation process. Chitin and chitosan are biopolymers obtained from crustacean shells of marine source, and they are non-toxic, biodegradable, and biocompatible[3,15,19]. The amino (–NH$_2$) groups in the chitosan polymer chain provide anti-bacterial, anti-fungal and anti-microbial properties without causing inflammatory reaction[15,20]. Chitosan-based composites are commonly used in medical technology as drug delivery systems, scaffold-based, wound healing, and tissue engineering materials[15]. Materials obtained from biogenic sources are attracting increasing interest due to remarkable biointeractive surface at cell level, better cell attachment and growth, and therefore, are more biocompatible than synthetic materials[3].

Considering all mentioned above, the aim of the present work was to synthesize biomimetic hydroxyapatite and prepare composite scaffolds based on chitosan. The preparation study and biological properties of chitosan/hydroxyapatite (CS/HAp) scaffolds have been studied, using three different biogenic sources for HAp preparation (hen eggshells, seashells and cuttlefish bone).

Materials and methods

Preparation of starting materials

Calcium oxide (CaO) obtained from synthetic (CaCO$_3$, TTT) and biogenic calcium carbonate from hen eggshell, cuttlefish bone (*Sepia officinalis* L.), and seashell (*Trachycardium egmontianum* L.) was used as the source of Ca^{2+} ions for HAp synthesis. To remove the organic matter and obtain CaO from hen eggshell (CaO_e), cuttlefish bone (CaO_c), and seashell (CaO_s), they were washed, crushed, and calcined at 700 °C in air atmosphere for 4 h[6,12]. Synthetic CaO was obtain by calcination at same conditions as synthetic CaCO$_3$.

Synthesis of hydroxyapatite

HAp was synthesised by wet precipitation method by dissolving the appropriate amounts of CaO from different sources (prepared as described in *Preparation of starting materials*) in distilled wa-

ter. Ammonium dihydrogen phosphate (NH$_4$H$_2$PO$_4$, Lachner) was added into solution to gain Ca/P molar ratio 1.67 (stoichiometric HAp). Stirring was continued for 3 days at 60 °C followed by overnight aging at room temperature. The synthesised HAp powders from CaO, CaO_e, CaO_c and CaO_s are referred to as HAp, HAp_e, HAp_c and HAp_s, respectively. Part of each sample was heat treated at 1200 °C for 2 h.

Preparation of chitosan-hydroxyapatite biocomposite scaffolds

The appropriate amount of chitosan was added to 0.40 wt% acetic acid solution to obtain 1.2 wt% chitosan solution at ambient temperature. The appropriate amounts of HAp, HAp_e, HAp_c, and HAp_s were added to obtain 30 wt% of HAp in chitosan solution, based on a previous study[21]. The CS/HAp suspensions were cooled to 4 °C, set in moulds, frozen, and kept at –30 °C for 8 h. Further, frozen samples were immersed into the neutralisation medium of 1 M NaOH/ethanol at –30 °C for 24 h to induce gelation of chitosan. The samples were rinsed in ethanol (96 wt%) at –30 °C for 24 h, washed with distilled water, frozen, and lyophilized. The synthesised chitosan/hydroxyapatite biocomposite scaffolds from HAp, HAp_e, HAp_c, and HAp_s are referred to as CS/HAp, CS/HAp_e, CS/HAp_c, and CS/HAp_s, respectively. Schematic diagram of composite scaffold preparation is shown in Fig 1.

Characterisation of obtained materials

Elemental analysis was performed by ICP-MS (ICP-MS PerkinElmer SCIEXT ELANR DRC-e, Concord, ON, Canada) according to the manufacturer's protocol. In each batch, ICP-MS accuracy was verified with standard reference materials with results within the certified concentration range for all relevant elements (ICP-MS Complete Standard-V-ICPMS-71A, Inorganic Ventures, USA). Each sample (100 mg) was dissolved in 1 mL of aqueous solution of HNO$_3$ (Ultra-Pure, Sigma Aldrich, St. Louis, Missouri, SAD), and the solution volume was increased up to 10 mL with ultrapure water.

The final pH of precipitated suspensions was measured on Schott CG 842 pH-meter using Blue-Line 14 electrode with precision of 0.01 at room temperature.

Phase analyses of obtained calcium oxides were done using X-ray diffraction analysis (XRD) performed on Shimadzu XRD-6000 (Shimadzu, XRD-6000, Duisburg, Germany) diffractometer with Cu K$_\alpha$ (1.5406 Å) radiation operated at 40 kV and 30 mA, in the range 35°–70°, at a step size of 0.02°, and exposure of 0.6 s. Phase analysis of
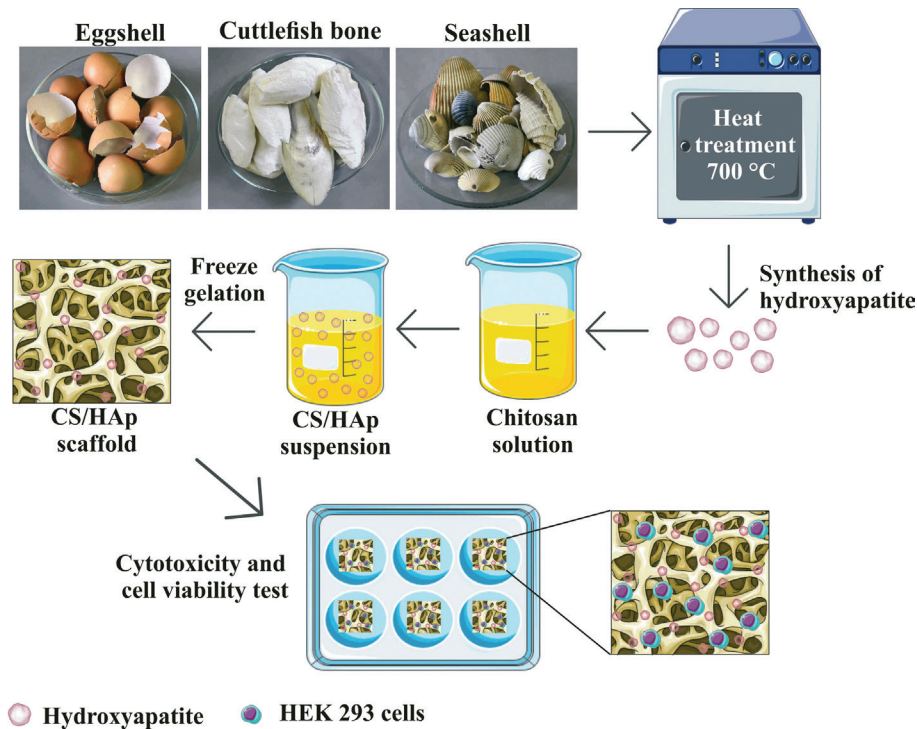
F i g . 1 – *Schematic diagram of the synthesis of composite chitosan/hydroxyapatite scaffolds obtained from eggshell, cuttlefish bone, and seashell*

as-prepared and heat-treated HAp powders, mixed with 5 wt% of polycrystalline silicon standard (NIST SRN 640e, Sigma Aldrich), was performed using X-ray diffraction analysis (XRD) in the range of 20°–70°, at a step size of 0.02°, and exposure of 3 s. The software DIFFRAC.SUITE TOPAS V.5.0. (Bruker, Karlsruhe, Germany) with the fundamental parameters approach was employed for Rietveld refinements. The structural parameters of HAp obtained by Veselinović *et al.*[22], β-tricalcium phosphate by Yashima *et al.*[23], and α-tricalcium phosphate by Mathew *et al.*[24], have been used as the initial values in the refinements. The crystallite size of HAp along the *c*- and *a*-axis were calculated applying Scherrer's approximation, measuring the full width at half maximum (FWHM) of reflection. The weighted profile R-factor (R_{wp}) was used to assess the goodness-of-fit of the Rietveld refinement, while results with R_{wp} < 11 % and R_{exp} < 3 % were considered to be acceptable.

The Fourier transform infrared spectra (FTIR) of as-prepared HAp powders and CS/HAp biocomposite scaffolds were recorded by attenuated total reflectance (ATR) spectrometer for solids with diamond crystal (Bruker, Vertex 70, Ettlingen, Germany) at 20 °C, over the spectral range of 4000–400 cm⁻¹, with 32 scans and 4 cm⁻¹ of resolution.

The morphology of prepared CS/HAp biocomposite scaffolds was analysed by scanning electron microscopy (SEM, TESCAN, Vega3 EasyProbe, Kohoutovice, Czech Republic) at electron beam energy of 11 keV. Scaffolds were coated with plasma of gold and palladium for 90 s. Obtained SEM images and ImageJ software (ImageJ2, Madison, Wisconsin, USA) were used to determine diameter of 350 pores of different CS/HAp scaffolds. The results are shown as pore density (%) of each pore range in relation to the total number of measured pores.

Porosity of the scaffolds was evaluated by Archimedes' principle, immersing each scaffold in ethanol (ρ = 0.789 g cm⁻³) at room temperature. The scaffolds porosity (%) was calculated as the pore volume (V_{pore}) fraction within the total volume of scaffold ($V_{CS/HAp}$) according to the Eq. (1):

$$\text{Porosity}\,(\%) = \frac{V_{pore}}{V_{CS/HAp}} \qquad (1)$$

The samples were cut with biopsy puncher into cylindrical pieces of 6 mm diameter (*D*) from previously prepared scaffold with uniform thickness (*H*) of ~1 mm. The dry samples (n = 5) were initially weighed (W_d). After immersion in ethanol under vacuum atmosphere, excess liquid was removed with the humid blanket, and samples were weighed again (W_e). The pore volume was calculated according to Eq. (2):

$$V_{pore} = \frac{W_e - W_d}{\rho_{ethanol}} \qquad (2)$$

The density of cylindrically-shaped scaffold is calculated according to Eq. (3)

$$\rho_{CS/HAp} = \frac{W_d}{\pi \cdot (D/2)^2 \cdot H} \qquad (3)$$

Biological evaluation

Cell seeding

Prepared scaffolds were cut into cylindrical pieces of 6 mm diameter and ~1 mm height, sterilised in 96 % ethanol for 24 h. After sterilisation, scaffolds were washed 3 times with phosphate-buffered saline (PBS) solution (Gibco – Thermo Fisher Scientific, Waltham, Massachusetts, USA), and left in Dulbecco's modified Eagle's culture medium (DMEM) – high glucose (Sigma- Aldrich, St. Louis, Missouri, USA) supplemented with 10 % foetal bovine serum (Capricorn Scientific, Ebsdorfergrund, Hessen, Germany) and 1 % penicillin/streptomycin (Lonza, Basel Switzerland) for 24 h at 4 °C. The following day, scaffolds were transported into polystyrene 96-well plates with hydrophobic surface (Corning – Sigma Aldrich).

The human embryonic kidney 293 (HEK 293) cells were seeded on each scaffold in a concentration $0.5 \cdot 10^5$ cells/200 µL of medium per well. Cell suspension was added on each scaffold, and incubated for 30 min in the incubator to allow cell attachment and migration inside the scaffold. Following the incubation period, the medium was added to a final volume of 200 µL per well. Each experiment was performed in triplicate. Blanks for both assays were included as well. The cells were kept in a 5 % CO_2 humidified atmosphere at 37 °C.

Cytotoxicity evaluation by MTT assay

Evaluation of potential cytotoxicity was obtained by staining with (3-(4,5-dimethylthiazol-2-yl)-2,5-diphenyltetrazolium bromide) (MTT, Sigma-Aldrich, St. Louis, Missouri, USA), and colorimetric detection at 560 nm using microplate reader (GlowMax-Multi, PromegaMadison, Wisconsin, USA) after 1 and 3 days of cell culture. The medium was removed, and 200 µL of MTT solution diluted in medium (0.5 mg mL^{-1}) was added to each well. Following the incubation period of 3 h at 37 °C, MTT solution was aspirated and 150 µL of DMSO (Sigma-Aldrich, St. Louis, Missouri, USA) added to each well. Following the 15 min incubation needed for dissolution of formazan crystals, 100 µL of solution was transferred into clean 96-plate in order to read absorbance.

Quantitative detection of cell viability by Live and Dead Cell assay

The percentage of live and dead cell population was determined by fluorescent detection using Live and Dead kit (Abcam, Cambridge, UK) after 1 and 7 days of cell culture. In order to collect cells from each scaffold, the medium was removed; scaffolds were washed with PBS followed by trypsinisation (Sigma-Aldrich, St. Louis, Missouri, USA) and neutralisation with the medium. Samples were centrifuged at 300 x g for 5 min, and the supernatant was removed. The cell pallet was washed with PBS and incubated with 200 µL of the stain diluted 1 000 x in PBS. After 10 min incubation in the dark, solution was transferred into black opaque 96-well plates (Corning – Sigma Aldrich, St. Louis, Missouri, USA) and analysed on microplate reader (GlowMax-Multi, PromegaMadison, Wisconsin, USA) using fluorescent filters (excitation 490 nm, emission 510–570 nm).

Statistical analysis

MTT experiments were performed in triplicate (n = 3), and Live and Dead assay in quadruplicate (n = 4). All data were expressed as mean ± standard deviation. Statistical analysis was performed using one-way ANOVA test followed by a post-hoc test to evaluate the statistical significance between groups. A value of $p < 0.05$ was considered statistically significant, and $p < 0.01$ was considered highly statistically significant.
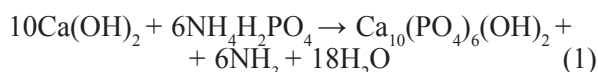
Results and discussion

Pharmacologics and biologics were used in combination with calcium phosphate ceramics (CaP) to increase bone regeneration. However, the use of growth factors might result in negative side effects, such as unwanted ectopic bone formation. The natural bone mineral is multi-substituted calcium-deficient apatite, which includes low concentrations of different ions, such as Mg^{2+}, Sr^{2+}, Na^+, CO_3^{2-}, Fe^{3+}, etc. Nowadays, the interest is turning to biomimetic synthetic apatite, where biogenic sources are used to produce multi-substituted HAp as an alternative and potentially safer strategy[3,25,26]. The trace elements are essential during bone tissue regeneration as they increase proliferation and differentiation of osteoblast cells, and decrease osteoclast cells activity[26]. Moreover, the presence of trace elements results in higher dissolution rate compared to stoichiometric hydroxyapatite. That leads to higher concentration of released ions that are essential for bone regeneration process[27]. According to *in vivo* studies obtained by Lee *et al.*[28], higher rate of bone formation was measured in defect filled with HAp obtained from eggshells compared to defect filled with HAp obtained from seashells. Different bone formation can be the result of different element composition of HAp obtained from different sourc-

es. Furthermore, recently developed interest for nanotechnology in many fields is producing interesting and imminent applications for nano-hydroxyapatite in orthopaedics[29], dentistry[30] and maxillofacial[31] surgery. The aim of this study was the synthesis of multi-substituted HAp, and to determine which of the biogenic sources and associated trace elements leads to enhanced biological performance. The HAp was prepared from biogenic waste materials that are available in large quantities in nature. Hen eggshell, seashell, and cuttlefish bone are mainly composed of calcium carbonate (~95 %), while the rest is organic component and mineral salts[32]. To mimic collagen type I in natural bone tissue, biopolymer chitosan as polymer matrix was used.

XRD patterns of calcium oxides

After the heat treatment of synthetic and biogenic calcium carbonates ($CaCO_3$), the XRD patterns (Fig. 2a) show characteristic peaks for CaO (ICDD 82-1691), without characteristic peaks of aragonite and calcite polymorphs. Under heating, $CaCO_3$ decomposes to calcium oxide (CaO) (and carbonate dioxide), which was further dissolved in distilled water, producing calcium hydroxide ($Ca(OH)_2$)[25,26]. To obtain HAp, appropriate amount of $NH_4H_2PO_4$ was added to $Ca(OH)_2$ and following reaction occurred[6]:

$$10Ca(OH)_2 + 6NH_4H_2PO_4 \rightarrow Ca_{10}(PO_4)_6(OH)_2 + {} + 6NH_3 + 18H_2O \qquad (1)$$

FTIR analysis

FTIR spectra (Fig. 2b) of all as-prepared powders (HAp, HAp_e, HAp_c, and HAp_s) is shown in the range 400–1550 cm^{-1}, while at the wave numbers >1550 cm^{-1} significant bands were not detected. Typical bands of phosphate (PO_4^{3-}) group at 1026 and 1091 cm^{-1} are attributed to asymmetric stretching vibration of P–O, bands at 561 cm^{-1} and 601 cm^{-1} to asymmetric bending vibrations of O–P–O and 961 cm^{-1} band associated to symmetric stretching vibration of P–O, which can be assigned to HAp phase. The absorption bending vibrations of O–H observed around 632 cm^{-1} is characteristic for structural OH– group in HAp crystal[34,35]. Weak absorption bands characteristic for carbonate (CO_3^{2-}) group at 870 (out of plane bending), 1416 and 1455 cm^{-1} (asymmetric stretching) indicate that tetrahedral PO_4^{3-} sites in the HAp lattice are partially replaced by CO_3^{2-} (B-type of substitution) typical for biological apatite[36,37]. As HAp powders are synthesised from CaO, CO_3^{2-} substitution was expected due to the high reactivity of the initial component and the presence of CO_2 in the process of synthesis
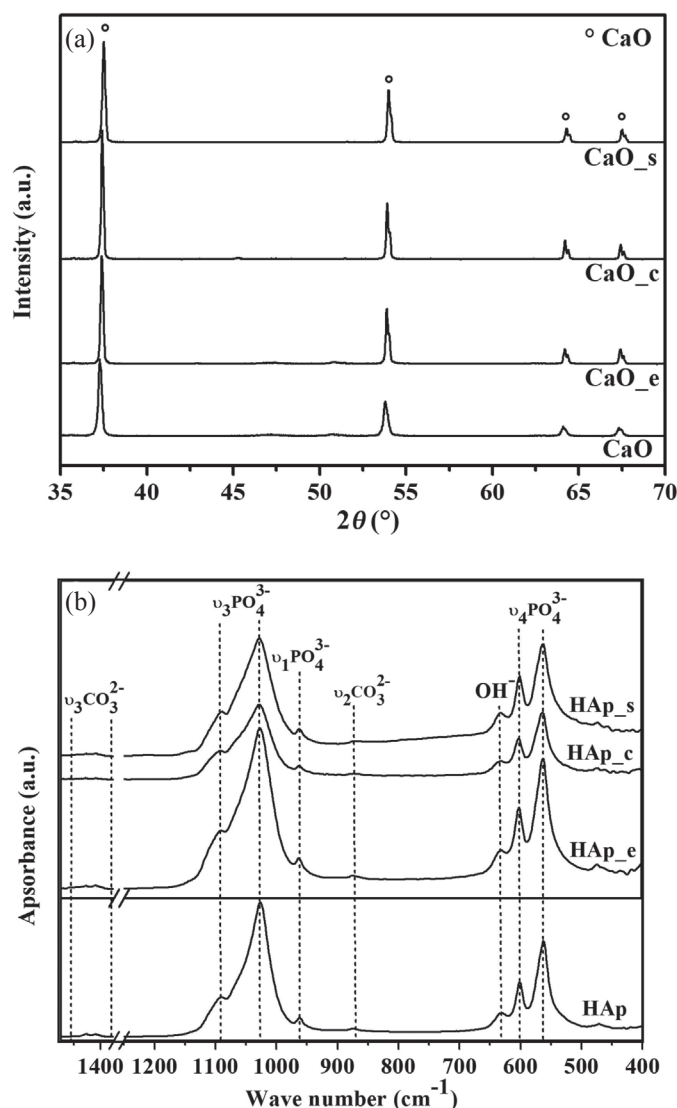

Fig. 2 – *XRD patterns (a) of heat-treated calcite (synthetic, CaO; eggshell, CaO_e; cuttlefish bone, CaO_e; seashell, CaO_s). Characteristic CaO (ICDD 82-1691) diffraction maxima are depicted as (°). FTIR spectra (b) of as-prepared HAp synthesised from prepared calcium oxides.*

at atmosphere conditions, as previously described by Goloshchapov *et al.*[32] The CO_3-substitution in HAp lattice enhances bioresorption and therefore osteogenic performance of synthetic material[32]. As reported by Kumar *et al.*[34], CO_3^{2-} ions are most abundant ions in natural bone mineral with weight ratio in the range 4–8 wt%. In the early stage of bone maturation, B-type substitution is dominant, while as humans grow older, A-type substitution increases[34].

Chemical composition of as-prepared powders

The chemical composition of HAp powders was determined by ICP-MS analysis (Table 1). In all prepared samples from biogenic source Sr^{2+}, Mg^{2+} and Na^+ ions, which are typical trace elements in natural bone mineral, were detected. Compared

T a b l e 1 – *Results of ICP-MS analysis and quantitative analysis of as-prepared CaP phases performed by Rietveld refinement of the XRD data*

Sample	Minor substituents (mol%)					Ca/P (mol mol⁻¹)	Quantitative analysis (wt%)	
	Sr	Na	Mg	Al	Fe		HAp	ACP
HAp_s	0.20	0.34	0.26	0.07	0.07	1.58	64.04	35.96
HAp_c	0.49	0.74	0.60	0.06	0.08	1.48	88.62	11.38
HAp_e	0.12	0.13	1.40	0.05	0.06	1.55	75.52	24.48
HAp	0.01	0.00	0.40	0.05	0.02	2.08	85.59	14.41

to HAp obtained from biogenic source (HAp_e, HAp_c, and HAp_s), control powder (HAp) prepared from synthetic CaO, had significantly lower content of strontium (0.01 mol%) and sodium ions (0.00 mol%), while comparable content of magnesium (0.40 mol%) ions. The sodium (0.74 mol%) and strontium (0.49 mol%) contents were significantly higher in the case of HAp_c, while higher magnesium content (1.40 mol%) was measured in HAp_e. The Sr^{2+}, Mg^{2+} and Na^+ content were significantly lower in the case of HAp_s compared to HAp_c and HAp_e. The higher magnesium content in HAp obtained from hen eggshells is not surprising since the hen eggshell is composed of $CaCO_3$, organic component, and ~1 % magnesium carbonate, as previously described by Akram *et al.*[10] These results are in accordance with the work of Lee *et al.*[28], who observed higher concentration of Mg ions in HAp obtained from eggshell compared to HAp obtained from seashells. The aragonite structure of cuttlefish bone is stabilised with strontium ions[38,39] that results in higher strontium content in HAp_c compared to HAp_e and HAp_s. Obtained results provide additional support for results obtained by previous studies confirming that by using biogenic sources, the multi-substituted hydroxyapatite can be obtained.

Sodium (Na^+) and magnesium (Mg^{2+}) ions are highly important in the early stage of bone mineralisation, whereas the lack of these ions may result in bone fragility[34]. Previous studies have shown that substituting CaP materials with Mg^{2+} improved densification as well as osteoblastic cellular attachment, proliferation, and alkaline phosphatase (ALP) production[26]. *In vivo* studies obtained by Landi *et al.*[40] showed greater osteogenic properties of CaPs substituted with Mg^{2+} compared to non-substituted system. Further, magnesium possesses antibacterial and antitumor properties reducing the risk of inflammatory reaction[41]. Strontium plays a crucial role in bone formation by increasing osteoblast activity through stimulating the calcium sensing receptor, while reducing bone resorption by inhibiting the formation of osteoclasts[26,42]. Compared to other scaffold materials that are combined with growth

factors, the scaffolds composed of hydroxyapatite substituted with trace elements can achieve long-term release of ions that promote bone repair, and show good bioactivity and osteoinductivity in terms of proliferation, cell viability, and morphology[42].

As expected, HAps synthesised from biogenic sources have lower Ca/P ratio (Table 1) than stoichiometric HAp with Ca/P molar ratio 1.67. This can be due to trace elements present in HAp structure as determined by ICP-MS method. Obtained results are in good agreement with bioapatite that is so-called calcium-deficient hydroxyapatite with Ca/P molar ratio ~1.5[43,44]. Contrary to expectations, the HAp obtained from synthetic CaO had Ca/P ratio 2.08, although the stoichiometric Ca/P ratio was expected. The reason for this rather contradictory result is still not entirely clear, but there are two possible explanations for this outcome. Comparing the experimental diffraction pattern (Fig. 3) to JCPDS standards, the crystalline phase is ascribed to HAp (JCPDS 09-0432), while Rietveld refinement studies demonstrated presence of amorphous calcium phosphate (ACP) phase as well (Table 1). The ACP can have Ca/P molar ration in the range 1.2–2.2, depending on the synthesis conditions and used precursors[43]. Further, the higher Ca/P molar ratio can be the result of higher calcium content and lower phosphate content as result of B-type substitution, as previously explained by FTIR analysis.

XRD patterns of as-prepared powders and Rietveld refinements

Comparison of the XRD results to JCPDS HAp standard, confirmed the formation of crystalline hexagonal structure in the space group $P6_3/m$. Rietveld refinement studies have confirmed the presence of ACP in all as-prepared samples. The weight percentage of ACP (Table 1) differed between the samples, 14.41 wt% was determined in HAp, 24.48 wt% in HAp_e, 11.38 wt% in HAp_c, 35.96 wt% in HAp_s, respectively. The final pH of all precipitated solutions at room temperature was 10.41 ± 0.06, and it favoured HAp and ACP precipitation[45]. In the literature, different estimates of the ACP content in bone mineral can be found, in the range 1–30 % of
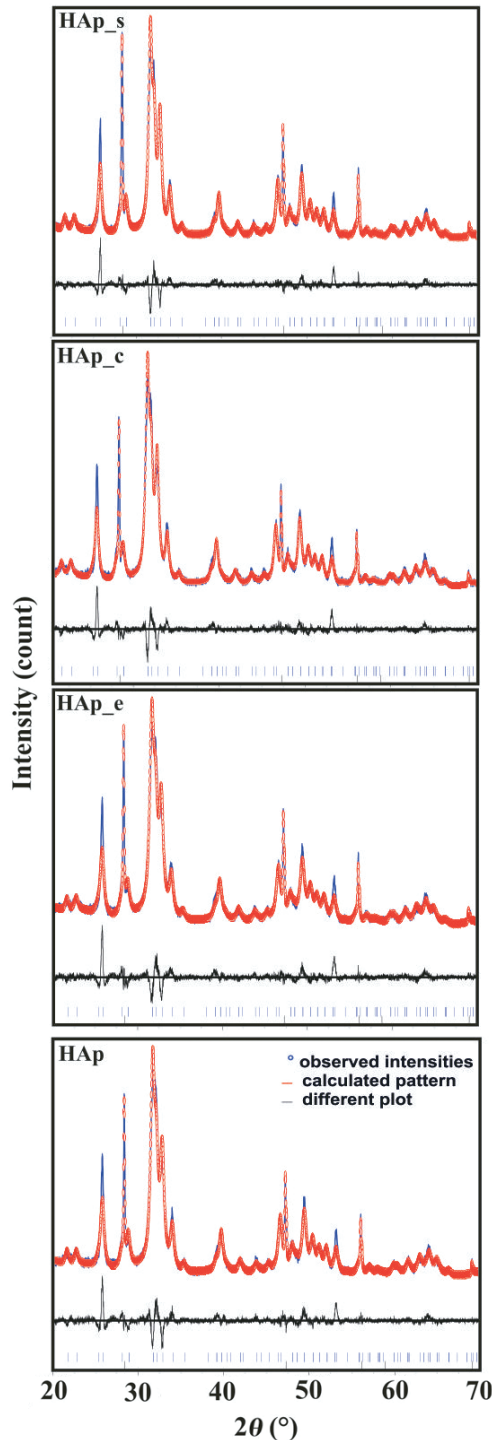
F i g . 3 – *Rietveld analysis pattern of powder diffraction data for as-prepared CaP powders obtained from different biogenic sources. The open circles are experimental data and the solid lines are calculated intensities. The difference between the experimental and calculated intensities is plotted below the profile ($R_{wp} < 11$ %; $R_{exp} < 3$ %). Bragg positions of hydroxyapatite and silicon (standard) are marked below each pattern.*

T a b l e 2 – *Unit cell parameters and crystal size of HAp in the as-prepared CaP powders*

Sample	HAp			
	$V(Å^3)$	$a = b(Å)$	$c(Å)$	$L(nm)$
HAp_s	530.084	9.4304265	6.8825875	13.93
HAp_c	529.946	9.4298413	6.8816424	13.03
HAp_e	529.956	9.4332978	6.8767361	10.99
HAp	529.730	9.4284543	6.8808578	12.21

T a b l e 3 – *Quantitative analysis of phases in heat-treated CaP powders performed by Rietveld refinement of the XRD data*

Sample	Quantitative analysis (wt%)			
	HAp	β-TCP	α-TCP	ACP
HAp_s_h	58.62	4.31	14.52	22.55
HAp_c_h	74.09	17.38	4.69	3.84
HAp_e_h	42.65	37.46	–	19.89
HAp_h	68.32	12.35	18.73	0.60

of HAp obtained from different sources (Table 2), and they were almost identical to lattice parameters of HAp standard JCPDS 09-0432. It can be assumed that the presence of trace elements had no influence on the cell structure of HAp. The average crystallite size (*L*), calculated using Scherrer equation, was 12.21 nm for HAp, 10.99 nm for HAp_e, 13.03 nm for HAp_c, and 13.39 nm for HAp_s. All prepared HAp powders could be considered as nanostructured, and the surface of nanostructured materials plays an important role in cell adhesion, migration, and extracellular matrix production[46].

XRD patterns of heat-treated powders and Rietveld refinements

XRD patterns of heat-treated powders at 1200 °C are presented in Fig. 4. The synthesised HAp, HAp_e, HAp_c, and HAp_s powders after heat treatment were referred to as HAp_h, HAp_e_h, HAp_c_h, and HAp_s_h, respectively. In comparison to XRD patterns of as-prepared powders, the diffraction peaks of heat-treated powders had sharpened, indicating an increase in crystallinity due to the heat treatment. The phase composition of samples after heat treatment is given in Table 3. HAp_h, HAp_c_h, and HAp_s_h were composed of HAp (JCPDS 09-0432), β-TCP (JCPDS 09-0169), α-TCP (JCPDS 09-0348) and ACP, while in HAp_e_h powder α-TCP was not detected. As previously described by Liao *et al.*[47], XRD patterns, after heat treatment of hydroxyapatite in range 1000 – 1350 °C, showed characteristic peaks of stoichiometric HAp.

the total mineral mass, while the rest is poorly crystalline calcium deficient hydroxyapatite substituted with various ions[45].

The Rietveld refinement studies revealed no significant difference between the lattice parameters
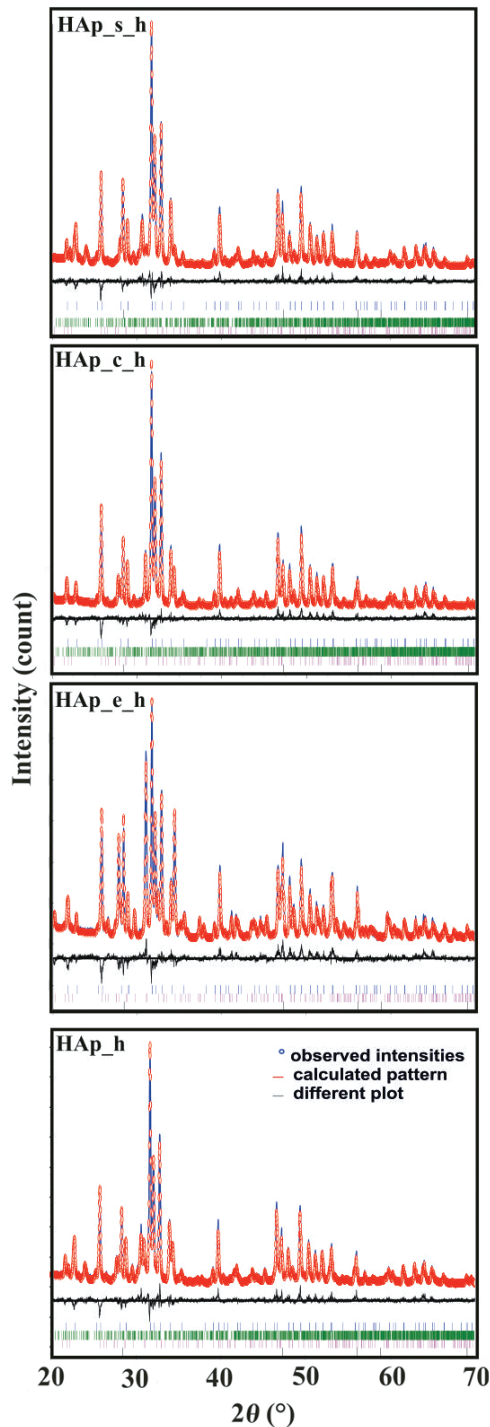
Fig. 4 – *Rietveld analysis pattern of powder diffraction data for heat-treated CaP powders obtained from different biogenic sources. The open circles are experimental data and the solid lines are calculated intensities. The difference between the experimental and calculated intensities is plotted below the profile (R_{wp} < 11 %; R_{exp} < 3 %). Bragg positions of hydroxyapatite, β-tricalcium phosphate, α-tricalcium phosphate and silicon (standard) are marked below each pattern.*

However, calcium deficient HAp with trace elements in its lattice structure can reduce the temperature of phase transformation to β-TCP and α-TCP due to disrupted crystal lattice stability[47]. The HAp_e, HAp_c, and HAp_s obtained from biogenic source were composed of calcium deficient HAp as Ca/P ratio was lower than 1.67, and partial phase transformation to β-TCP and α-TCP was expected. The HAp_e_h was composed of HAp and β-TCP without precipitation of α-TCP. Stipniece *et al.*[48] reported that Mg^{2+} ions promote the thermal conversion of HAp to β-TCP, i.e., those ions prefer to substitute and stabilise β-TCP crystal structure. It can be supposed that high concentration of Mg^{2+} ions in HAp_e is the reason why HAp to α-TCP transformation had not been observed. Similar effect was detected in HAp_c_h, where higher amount of precipitated β-TCP and lower amount of α-TCP was detected compared to HAp_h and HAp_s_h due to 0.60 mol% substitution with Mg^{2+} ion prior to heat treatment.

Morphology of CS/HAp scaffolds

The microstructures of CS/HAp, CS/HAp_e, CS/HAp_c, and CS/HAp_s shown in Fig. 5a reveal highly porous structure with sphere-like HAp particles homogeneously dispersed in chitosan matrix. In natural bone tissue, the mineral is mainly calcium deficient carbonate HAp substituted with trace elements with plate-like morphology. However, synthetic HAp can have various nanostructures like sphere, rod, plate, flake, flower, etc.[6]

The determined pore volume fraction was 57.02 ± 0.01 % in CS/HAp, 60.81 ± 0.09 % in CS/HAp_e, 60.24 ± 0.07 % in CS/HAp_c, 58.41 ± 0.04 % in CS/HAp_s scaffold, respectively. Highly porous structure is an essential parameter for oxygen, nutrients and metabolic waste diffusion, and enables tissue ingrowth and contributes to the creation of permanent interactions between a tissue and the implant[18,49]. The analysis of porosity and pore size distribution revealed no significant differences between the samples. The distribution of pore size, shown in Fig. 5b, ranged from ~35 to ~350 μm in the CS/HAp_e, CS/HAp_c, and CS/HAp_s scaffolds, and from ~50 to ~400 μm in CS/HAp scaffold. It has been suggested that the pore size must be large enough to allow migration of cells, but small enough to allow the binding of cells to the scaffold. Porous polymer scaffolds with a pore size of 100–500 μm, combined with hydroxyapatite, were found to be optimal scaffolds for bone-tissue engineering[49]. It can be assumed that only different trace elements present in HAp lattice would influence biological properties of obtained scaffolds.

FTIR analysis of CS/HAp scaffolds

FTIR spectra (Fig. 6) of composite scaffolds (CS/HAp, CS/HAp_e, CS/HAp_c, and CS/HAp_s) and control (CS) is shown in the range 400–1750 cm^{-1},

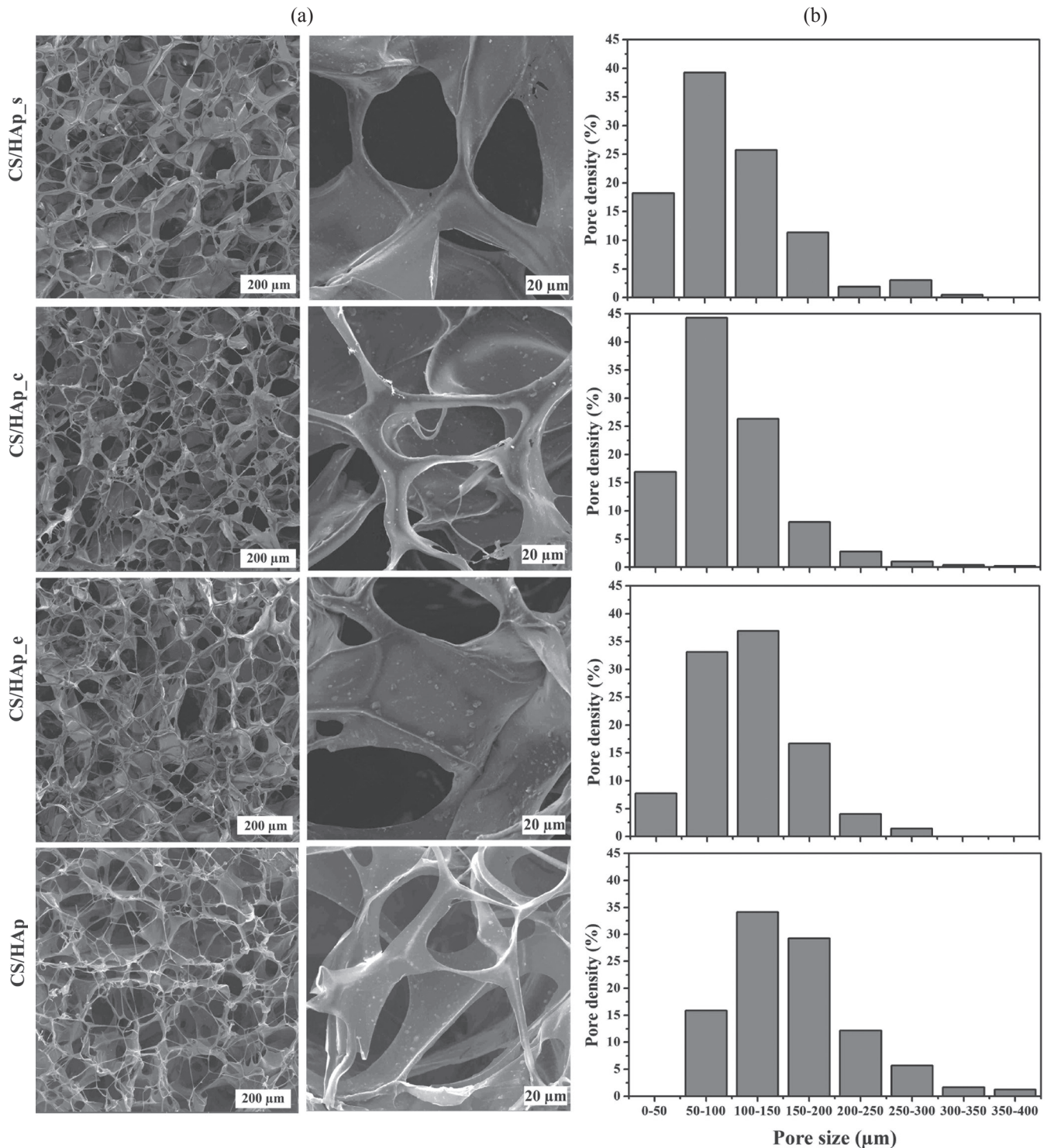(a)   (b)

F i g . 5 – *Microscopic imaging (a) and pore size distribution (b) of prepared composite scaffolds obtained from different biogenic sources. Scale bar: 200 and 20 μm.*

as at the wave numbers >1750 cm⁻¹ significant bands were not found. Typical bands of chitosan groups were found at 1654 cm⁻¹, corresponding to amid I (carbonyl band of amid), at 1568 cm⁻¹ attributed to amid II (amino band of amid), 1421 cm⁻¹ and 1323 cm⁻¹ that correspond to the vibrations of OH and CH in the ring, 1377 cm⁻¹ to CH_3 in amide group, and range 1025 – 1151 cm⁻¹ to C–O–C in glycosidic linkage[50]. Along with characteristic bands

for chitosan, typical bands for HAp were found at 564 cm⁻¹, 600 cm⁻¹ and 1028 cm⁻¹ corresponding to PO_4^{3-}, and at 631 cm⁻¹ corresponding to OH⁻ group.

Biological evaluation of CS/HAp scaffolds

The biological evaluation of CS/HAp scaffolds has been performed on the HEK 293 cells to determine cytotoxicity and cell viability performance.

Mitochondria are essential metabolic organelles of cells, and their activity can be a direct indicator of cell viability and proliferation. MTT assay is used to assess the mitochondrial activity of cells. The viability of HEK 293 cells cultured on CS/HAp, CS/HAp_e, CS/HAp_c, and CS/HAp_s scaffolds was determined by MTT assay (Fig. 7a). The cells seeded on prepared scaffolds showed no significant difference in cell viability after 1 day of cell culture. Following the 3-day incubation period, the cell viability enhanced with significant difference for the cells seeded on CS/HAp_e, CS/HAp_c, and CS/HAp_s scaffolds, respectively. Meanwhile, the cells seeded on CS/HAp showed a lack of significant increase in cell viability. The significant increase in cell viability provides additional support for using biogenic sources as precursors to obtain scaffolds for bone regeneration.

The *Live/dead* assay was determined after 1 and 7 days of cell culture, and is shown in Fig. 7b. The composite scaffolds obtained from chitosan and HAp derived from biogenic sources (CS/HAp_e, CS/HAp_c an CS/HAp_s) displayed enhanced percent of live cells compared to the scaffold obtained from chitosan and synthetic hydroxyapatite (CS/HAp). The CS/HAp_e and CS/HAp_c showed greater percent of live cells after 7 days of cell culture compared to CS/HAp and CS/HAp_s, respectively.

Our results are in accordance with the work of Kim *et al.*[51] suggesting that cell proliferation is significantly higher for HAp obtained from cuttlefish bone compared to synthetic HAp. Similar findings are reported by Lee *et al.*[28] demonstrating better biological performance of HAp obtained from eggshells compared to seashells. As explained, the higher concentration of Mg^{2+} ions in HAp structure obtained from eggshells might be related to the higher bone regeneration in comparison with HAp obtained from seashells. The Mg^{2+} ions are related to the early stage of bone formation and metabolism. Both *in vitro* and *in vivo* studies show greater bone formation of materials enriched with Mg^{2+} ions[37,50]. Greater cell proliferation of the CS/HAp_c scaffold can be related to the higher content of Sr^{2+} ion as previously described by Braux *et al.*[52] and Neves *et al.*[53] The Sr^{2+} ions are used in osteoporosis treatment, and stimulate bone formation and decrease bone resorption *in vivo*. Lower cell viability on CS/HAp_s can be the result of a significantly lower trace element concentration of HAp obtained from seashells compared to HAp obtained from eggshells and cuttlefish bone.

Conclusion

Composite scaffolds based on biodegradable polymers and bioactive ceramics are promising materials for bone-tissue regeneration applications.
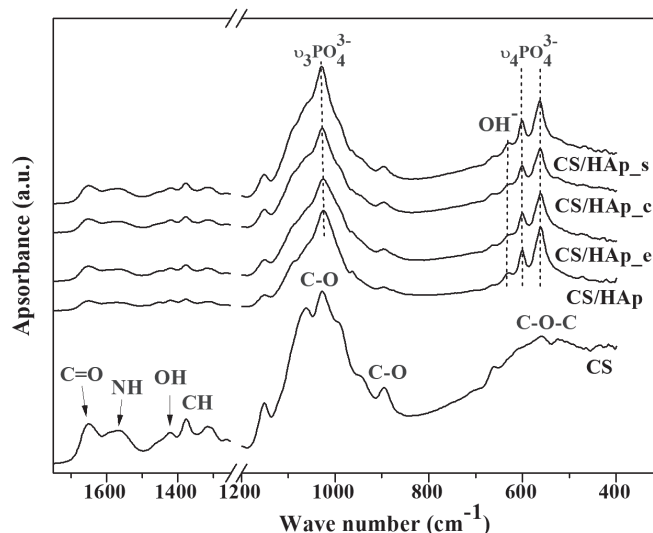

F i g . 6 – *FTIR spectra of prepared composite scaffolds obtained from different biogenic sources. Chitosan (CS) scaffold was used as a control.*
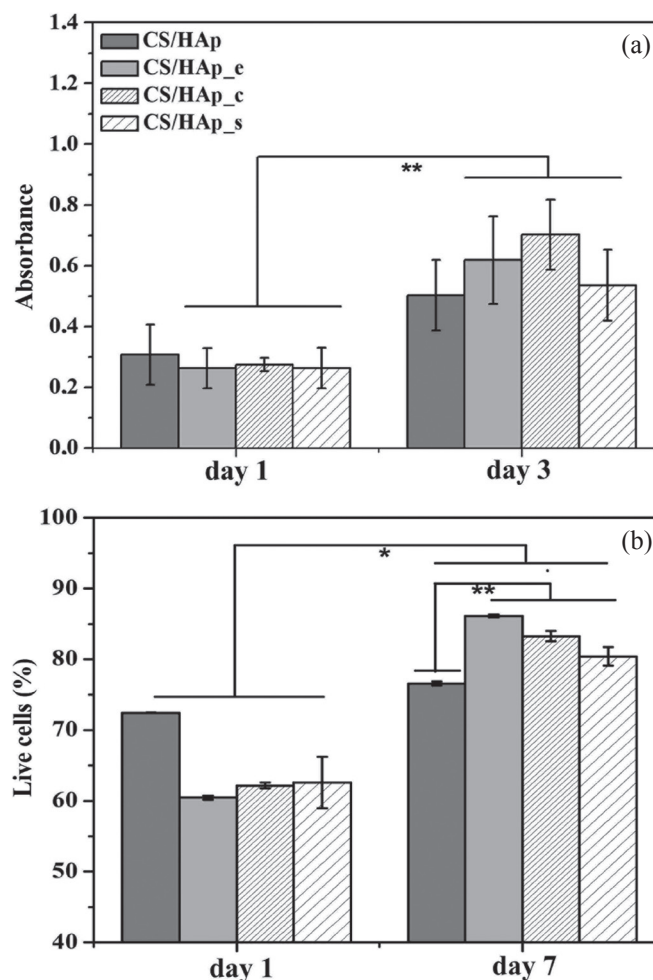

F i g . 7 – *Cytotoxicity (a) of CS/HAp scaffolds obtained from different biogenic sources. The viability of human embryonic kidney 293 cells at 1 and 3 days of cell culture expressed by the absorbance at 560 nm. Quantification (%) of live cells (b) on prepared scaffolds (CS/HAp, CS/HAp_e, CS/HAp_c, CS/ HAp_e) determined by Live/dead assay. The significant difference between two groups: * (p < 0.05), ** (p < 0.01).*

The incorporation of metal ions into a hydroxyapatite structure is a promising pathway to increase the biological properties of the scaffolds. Using biogenic sources, such as eggshells and cuttlefish bone, to prepare multi-substituted HAp, can be considered an environmentally friendly and economically viable approach. Positive influence of Mg^{2+} and Sr^{2+} ions, present in eggshell and cuttlefish bone, on cell viability has been observed. However, further studies involving swelling and biodegradation assay at simulated biological conditions, and seeding of stem or preosteoblastic lineage need to be performed in order to confirm CS/HAp_e and CS/HAp_c scaffolds as potential bone-tissue engineering materials.

Literature

1. *Mondal, S., Pal, U., Dey, A.,* Natural origin hydroxyapatite scaffold as potential bone tissue engineering substitute, Ceram. Int. **42** (2016) 18338.
   doi: https://doi.org/10.1016/j.ceramint.2016.08.165

2. *Lilley, K. J., Gbureck, U., Wright, A. J., Farrar, D. F., Barralet, J. E.,* Cement from nanocrystalline hydroxyapatite: Effect of calcium phosphate ratio, J. Mater. Sci: Mater. Med. **16** (2005) 1185.
   doi: https://doi.org/10.1007/s10856-005-4727-2

3. *Lalzawmliana, V., Anand, A., Mukherjee, P., Chaudhuri, S., Kundu, B., Nandi, S. K., Thakur, N. L.,* Marine organisms as a source of natural matrix for bone tissue engineering, Ceram. Int. **45** (2019) 1469.
   doi: https://doi.org/10.1016/j.ceramint.2018.10.108

4. *Cortesini, R.,* Stem cells, tissue engineering and organogenesis in transplantation, Transpl. Immunol. **15** (2005) 81.
   doi: https://doi.org/10.1016/j.trim.2005.09.013

5. *Sato, K.,* Mechanism of hydroxyapatite mineralization in biological systems, J. Ceram. Soc. Jpn. **115** (2007) 124.
   doi: https://doi.org/10.2109/jcersj.115.124

6. *Sadat-Shojai, M., Khorasani, M. T., Dinpanah-Khoshdargi, E., Jamshidi, A.,* Synthesis methods for nanosized hydroxyapatite with diverse structures, Acta. Biomater. **9** (2013) 7591.
   doi: https://doi.org/10.1016/j.actbio.2013.04.012

7. *Zhou, H., Lee, J.,* Nanoscale hydroxyapatite particles for bone tissue engineering, Acta. Biomater. **7** (2011) 2769.
   doi: https://doi.org/10.1016/j.actbio.2011.03.019

8. *Legeros, R. Z.,* Biodegradation and bioresorption of calcium phosphate ceramics, Clin. Mater. **14** (2013) 65.
   doi: https://doi.org/10.1016/0267-6605(93)90049-D

9. *Ho, W. F., Hsu, H. C., Hsu, S. K., Hung, C. W., Wu, S. C.,* Calcium phosphate bioceramics synthesized from eggshell powders through a solid state reaction, Ceram. Int. **39** (2013) 6467.
   doi: https://doi.org/10.1016/j.ceramint.2013.01.076

10. *Akram, M., Ahmed, R., Shakir, I., Ibrahim, W. A. W., Hussain R.,* Extracting hydroxyapatite and its precursors from natural resources, J. Mater. Sci. **49** (2014) 1461.
    doi: https://doi.org/10.1007/s10853-013-7864-x

11. *Lin, K., Zhou, Y., Zhou, Y., Qu, H., Chen, F., Zhu, Y., Chang, J.,* Biomimetic hydroxyapatite porous microspheres with co-substituted essential trace elements: Surfactant-free hydrothermal synthesis, enhanced degradation and drug release, J. Mater. Chem. **21** (2011) 16558.
    doi: https://doi.org/10.1039/C1JM12514A

12. *Kamalanathan, P., Ramesh, S., Bang, L. T., Niakan, A., Tan, C. Y., Purbolaksono, J., Chandran, H., Teng, W. D.,* Synthesis and sintering of hydroxyapatite derived from eggshells as a calcium precursor, Ceram. Inter. **40** (2014) 16349.
    doi: https://doi.org/10.1016/j.ceramint.2014.07.074

13. *Boutinguiza, M., Pou, J., Comesaña, R., Lusquiños, F., de Carlos, A. León, B.,* Biological hydroxyapatite obtained from fish bones, Mater. Sci. Eng. C **32** (2012) 478.
    doi: https://doi.org/10.1016/j.msec.2011.11.021

14. *Suresh Kumar, G., Girija, E. K.,* Flower-like hydroxyapatite nanostructure obtained from eggshell: A candidate for biomedical applications, Ceram. Inter. **39** (2013) 8293.
    doi: https://doi.org/10.1016/j.ceramint.2013.03.099

15. *Trakoolwannachai, V., Kheolamai, P., Ummartyotin, S.,* Development of HAp from eggshell waste and a chitosan based composite: In vitro behavior of human osteoblast-like cell (Saos-2) cultures, Int. J. Biol. Macromol. **134** (2019) 557.
    doi: https://doi.org/10.1016/j.ijbiomac.2019.05.004

16. *Rodríguez-Vázquez, M., Vega-Ruiz, B., Ramos-Zúñiga, R., Saldaña-Koppel, D. A., Quiñones-Olvera, L. F.,* Chitosan and its potential use as a scaffold for tissue engineering in regenerative medicine, Biomed. Res. Int. **2015** (2015) 821279.
    doi: https://doi.org/10.1155/2015/821279

17. *Szcześ, A., Hołysz, L., Chibowski, E.,* Synthesis of hydroxyapatite for biomedical applications, Adv. Colloid. Interface. Sci. **249** (2017) 321.
    doi: https://doi.org/10.1016/j.cis.2017.04.007

18. *Sobczak – Kupiec, A., Pluta, K., Drabczyk, A., Włos, M., Tyliszczak, B.,* Synthesis and characterization of ceramic – polymer composites containing bioactive synthetic hydroxyapatite for biomedical applications, Ceram. Inter. **44** (2018) 13630.
    doi: https://doi.org/10.1016/j.ceramint.2018.04.199

19. *Rezwan, K., Chen, Q. Z., Blaker, J. J., Boccaccini, A. R.,* Biodegradable and bioactive porous polymer/inorganic composite scaffolds for bone tissue engineering, Biomaterials **27** (2006) 3413.
    doi: https://doi.org/10.1016/j.biomaterials.2006.01.039

20. *Pillai, C. K. S., Paul, W., Sharma, C. P.,* Chitin and chitosan polymers: Chemistry, solubility and fiber formation, Prog. Polym. Sci. **34** (2009) 641.
    doi: https://doi.org/10.1016/j.progpolymsci.2009.04.001

21. *Rogina, A., Rico, P., Gallego Ferrer, G., Ivanković, M., Ivanković, H.,* In Situ hydroxyapatite content affects the cell differentiation on porous chitosan/ hydroxyapatite scaffolds, Ann. Biomed. Eng. **44** (2015) 1107.
    doi: https://doi.org/10.1007/s10439-015-1418-0

22. *Veselinović, Lj., Karanović, Lj., Stojanović, Z., Bračko, I., Marković, S., Ignjatović, N. Uskoković, D.,* Crystal structure of cobalt-substituted calcium hydroxyapatite nanopowders prepared by hydrothermal processing, J. Appl. Cryst. **43** (2010) 320.
    doi: https://doi.org/10.1107/S0021889809051395

23. *Yashima, M., Sakai, A., Kamiyama, T., Hoshikawa, A.,* Crystal structure analysis of β-tricalcium phosphate $Ca_3(PO_4)_2$ by neutron powder diffraction, J. Solid. State. Chem. **175** (2003) 272.
doi: https://doi.org/10.1016/S0022-4596(03)00279-2

24. *Mathew, M., Brown, W. E., Schroeder, L. W., Dickens, B.,* The crystal structure of alpha-$Ca_3(PO_4)_2$, Acta Crystallogr. B **33** (1977) 1325.
doi: https://doi.org/10.1107/S0567740877006037

25. *Salma-Ancane, K., Stipniece, L., Irbe, Z.,* Effect of biogenic and synthetic starting materials on the structure of hydroxyapatite bioceramics, Ceram. Inter. **42** (2016) 9504.
doi: https://doi.org/10.1016/j.ceramint.2016.03.028

26. *Bose, S., Fielding, G., Tarafder, S., Bandyopadhyay, A.,* Understanding of dopant-induced osteogenesis and angiogenesis in calcium phosphate ceramics, Trends Biotechnol. **31** (2013) 594.
doi: https://doi.org/10.1016/j.tibtech.2013.06.005

27. *Ressler, A., Cvetnić, M., Antunović, M., Marijanović, I., Ivanković, M., Ivanković, H.*, Strontium substituted biomimetic calcium phosphate system derived from cuttlefish bone, J. Biomed. Mater. Res. **108B** (2020) 1697-1709.
doi: https://doi.org/10.1002/jbm.b.34515

28. *Lee, S. W., Balázsi, C., Balázsi, K., Seo, D. H., Kim, H. S., Kim, C. H., Kim, S. G.,* Comparative study of hydroxyapatite prepared from seashells and eggshells as a bone graft material, J. Tissue. Eng. Regen. Med. **11** (2014) 113.
doi: https://doi.org/10.1007/s13770-014-0056-1

29. *Song, Y., Wu, H., Gao, Y., Li, J., Lin, K., Liu, B., Lei, X., Cheng, P., Zhang, S., Wang, Y., Sun, J., Bi, L., Pei, G.,* Zinc silicate/nano-hydroxyapatite/collagen scaffolds promote angiogenesis and bone regeneration via the p38 MAPK pathway in activated monocytes, ACS Appl. Mater. Interfaces **12** (2020) 16058.
doi: https://doi.org/10.1021/acsami.0c00470

30. *Scribante, A., Dermenaki Farahani, M. R., Marino, G., Matera, C., Rodriguez, Y., Baena, R., Lanteri, V., Butera, A.,* Biomimetic effect of nano-hydroxyapatite in demineralized enamel before orthodontic bonding of brackets and attachments: Visual, adhesion strength, and hardness in in vitro tests, Biomed. Res. Int. **2020** (2020) 2314.
doi: https://doi.org/10.1155/2020/6747498

31. *Khaled, H., Atef, M., Hakam, M.,* Maxillary sinus floor elevation using hydroxyapatite nano particles vs tenting technique with simultaneous implant placement: A randomized clinical trial, Clin. Implant. Dent. Relat. Res. **21(6)** (2019) 1241.
doi: https://doi.org/10.1111/cid.12859

32. *Goloshchapov, D. L., Kashkarov, V. M., Rumyantseva, N. A., Seredin, P. V., Lenshin, A. S., Agapov, B. L., Domashevskaya, E. P.,* Synthesis of nanocrystalline hydroxyapatite by precipitation using hen's eggshell, Ceram. Inter. **39** (2013) 4539.
doi: https://doi.org/10.1016/j.ceramint.2012.11.050

33. *Mohd Pu'ad, N. A. S., Koshy, P., Abdullah, H. Z., Idris, M. I., Lee, T. C.,* Syntheses of hydroxyapatite from natural sources, Heliyon **5** (2019) e01588.
doi: https://doi.org/10.1016/j.heliyon.2019.e01588

34. *Kumar, G. S., Girija, E. K., Venkatesha, M., Karunakaran, G., Kolesnikov, E., Kuznetsov, D.,* One step method to synthesize flower-like hydroxyapatite architecture using mussel shell bio-waste as a calcium source, Ceram. Inter. **43** (2017) 3457.
doi: https://doi.org/10.1016/j.ceramint.2016.11.163

35. *Sathiskumar, S., Vanaraj, S., Sabarinathan, D., Bharath, S., Sivarasan, G., Arulmani, S., Preethi, K., Ponnusamy, V. K.,* Green synthesis of biocompatible nanostructured hydroxyapatite from Cirrhinus mrigala fish scale – A biowaste to biomaterial, Ceram. Inter. **45** (2019) 7804.
doi: https://doi.org/10.1016/j.ceramint.2019.01.086

36. *Gibson, I. R., Bonfield, W.,* Novel synthesis and characterization of an AB-type carbonate-substituted hydroxyapatite, J. Biomed. Mater. Res. **59** (2002) 697.
doi: https://doi.org/10.1002/jbm.10044

37. *Lafon, J. P., Champion, E., Bernache-Assollant, D.,* Processing of AB-type carbonated hydroxyapatite $Ca_{10-x}(PO_4)_{6-x}(OH)_{2-x-2y}(CO_3)_y$ ceramics with controlled composition, J. Eur. Ceram. Soc. **28** (2008) 139.
doi: https://doi.org/10.1016/j.jeurceramsoc.2007.06.009

38. *Birchall, J. D., Thomas, N. L.,* On the architecture and function of cuttlefish bone, J. Mater. Sci. **18** (1983) 2081.
doi: https://doi.org/10.1007/BF00555001

39. *Hewitt, R. A.,* Analysis of aragonite from the cuttlefish bone of *Sephia officinalis* L., Mar. Geol. **18** (1975) M1.
doi: https://doi.org/10.1016/0025-3227(75)90033-X

40. *Landi, E., Logroscino, G., Proietti, L., Tampieri, A., Sandri, M., Sprio, S.,* Biomimetic Mg-substituted hydroxyapatite: From synthesis to in vivo behaviour, J. Mater. Sci. Mater. Med. **19** (2008) 239.
doi: https://doi.org/10.1007/s10856-006-0032-y

41. *Sabet, A. S., Jabbari, A. H., Sedighi, M.,* Microstructural properties and mechanical behavior of magnesium/hydroxyapatite biocomposite under static and high cycle fatigue loading, J. Compos. Mater. **0** (2017) 1.
doi: https://doi.org/10.1177/0021998317731822

42. *Zhang, X., Chen, Y., Han, J., Mo, J., Dong, P., Zhuo, Y., Feng, Y.,* Biocompatible silk fibroin/carboxymethyl chitosan/strontium substituted hydroxyapatite/cellulose nanocrystal composite scaffolds for bone tissue engineering, Int. J. Biol. Macromol. **136** (2019) 1247.
doi: https://doi.org/10.1016/j.ijbiomac.2019.06.172

43. *Boanini, E., Gazzano, M., Bigi, A.,* Ionic substitutions in calcium phosphates synthesized at low temperature, Acta Biomater. **6** (2010) 1882.
doi: https://doi.org/10.1016/j.actbio.2009.12.041

44. *Chen, Y. H., Tai, H. Y., Fu, E., Don, T. M.,* Guided bone regeneration activity of different calcium phosphate/chitosan hybrid membranes, Int. J. Biol. Macromol. **126** (2019) 159.
doi: https://doi.org/10.1016/j.ijbiomac.2018.12.199

45. *Dorozhkin, S. V.,* Amorphous calcium (ortho)phosphates, Acta Biomater. **6** (2010) 4457.
doi: https://doi.org/10.1016/j.actbio.2010.06.031

46. *Rogina, A., Antunović, M., Milovac, D.,* Biomimetic design of bone substitutes based on cuttlefish bone-derived hydroxyapatite and biodegradable polymers, J. Biomed. Mater. Res. B Appl. Biomater. **107** (2019) 197.
doi: https://doi.org/10.1002/jbm.b.34111

47. *Liao, C. J., Lin, F. H., Chen, K. S., Sun, J. S.,* Thermal decomposition and reconstruction of hydroxyapatite in air atmosphere, Biomed. Sci. Instrum. **35** (1999) 99.
doi: https://doi.org/10.1016/s0142-9612(99)00076-9

48. *Stipniece, L., Salma-Ancane, K., Borodajenko, M., Sokolova, M., Jakovlevs, D., Berzina-Cimdina, L.,* Characterization of Mg-substituted hydroxyapatite synthesized by wet chemical method, Ceram. Int. **40** (2014) 3261.
doi: https://doi.org/10.1016/j.ceramint.2013.09.110

49. *Chocholata, P., Kulda, V., Babuska, V.,* Fabrication of scaffolds for bone-tissue regeneration, Materials **12** (2019) 568.
doi: https://doi.org/10.3390/ma12040568

50. *Pawlak, A., Mucha, M.,* Thermogravimetric and FTIR studies of chitosan blends, Thermochim. Acta **396** (2003) 153.
doi: https://doi.org/10.1016/S0040-6031(02)00523-3

51. *Kim, B. S., Kang, H. J., Yang, S. S., Lee, J.,* Comparison of in vitro and in vivo bioactivity: Cuttlefish-bone-derived hydroxyapatite and synthetic hydroxyapatite granules as a bone graft substitute, Biomed. Mater. **9** (2014) 025004.
doi: https://doi.org/10.1088/1748-6041/9/2/025004

52. *Braux, J., Velard, F., Guillaume, C., Bouthors, S., Jallot, E., Nedelec, J. M., Laurent- Maquin, D., Laquerrière, P.,* A

new insight into the dissociating effect of strontium on bone resorption and formation, Acta Biomater. **7** (2011) 2593.
doi: https://doi.org/10.1016/j.actbio.2011.02.013

53. *Neves, N., Linhares, D., Costa, G., Ribeiro, C. C., Barbosa, M. A.,* In vivo and clinical application of strontium-enriched biomaterials for bone regeneration: A systematic review, Bone Joint. Res. **6** (2017) 366.
doi: https://doi.org/10.1302/2046-3758.66.BJR-2016-0311.R1